A dimensional case study of upper-tropospheric wind affects on a Florida cirrus anvil

Nicole Hastings, University of Wyoming

Abstract

Improvements to the modeling of upper-tropospheric anvil cirrus on the climate system requires a comprehensive view of anvils ranging from their physical dimensions and detailed microphysical properties to the dynamical processes producing and affecting them. Using data collected in 2002 from NASA's CRYSTAL-FACE campaign in Florida, a study of the physical effects of upper level winds and the advection of anvil cirrus was conducted. The focus of this analysis was to further our understanding of the affects of environmental conditions on the movement of particles within the cloud.

1. Introduction

Upper-tropospheric anvil cirrus are least understood in terms of the environmental and radiative energy feedbacks yet they are the most common clouds observed in the tropics and mid-latitude summers. The international satellite cloud climatology project (ISCCP) was established in 1982 and has been used to collect measurements in order to infer the global distribution of clouds. According to eight years of global statistics presented by Wylie et al. (1999), cirrus cover approximately 43% of the globe with the greatest coverage at low latitudes in the ITCZ region. A view of the average ice cloud fraction and it's location on the Earth derived from ISCCP data by Yost et al. can be seen in figure 1. Although all cirrus are formed by an uplift of moist air into high altitudes, over 50% of cirrus are directly associated to deep convective cumulonimbus in the tropical and subtropical latitudes.

The effect of cirrus on the climate relies upon the balance between the energy absorbed and the radiative scattering of the cloud. Cirrus can create warming anomalies by trapping longwave radiation due to their high altitudes and corresponding cold temperatures; refer to the Stephan-Boltzmann law, $E = \sigma T^4$ or more generally, the emmisivity of an object is proportional to the temperature of that object to the fourth power. Cirrus can inversely create cooling anomalies that are dependent on the size and concentration of ice crystals reflecting and scattering incoming shortwave radiation.

The areas affected by the radiative impacts of anvil cirrus are related directly to the convection intensity and the wind speed and direction at different levels within the cloud. A greater amount of convection will increase the amount of warm moist air into the cool upper levels of the troposphere creating a cloud with more particles per unit area and a higher optical thickness, thus creating a cooling effect. The speed and direction of the wind at different levels will significantly affect the horizontal coverage of the cloud as well as the vertical thickness of the layers themselves. The more spread an anvil experiences, the thinner it may become changing the radiative affects from a cooling trend to a warming anomaly. The dispersion of the particles to further areas will subsequently increase the amount of area affected by the upper level warming.

Several platforms have been launched to study and detect clouds: CloudSat – a polar orbiting 94GHz radar (Stephens et al., 2008), CALIPSO – a polar orbiting dual-wavelength (1064nm and 532nm) polarization-sensitive lidar (NASA CALIPSO, web), and GOES – a geostationary satellite equipped with a visible and infrared imaging system. Temporal issues arise when attempting to view a particular cloud mass over a short time using data sets collected by polar orbiting satellites. The cloud radar system (CRS) and the cloud polarization lidar (CPL) were engineered similar to CloudSat and CALIPSO respectively but can be attached to a research aircraft in order to gather data over one particular area and view the cloud as it changes over a smaller time scale.

The CRS and CPL were flown on the NASA ER-2 high altitude aircraft during the CRYSTAL-FACE campaign in southern Florida during the summer of 2002. CRYSTAL-FACE provided data of in situ hydrometeor size, shape and associated locations, atmospheric chemistry and aerosol as well as offering integrated cloud products from 3 different research platforms: satellite, airborne and ground-based systems. The observations made during this campaign offer important data for studying sub-tropical anvil clouds (NASA CRYSTAL-FACE, Web).

Data from the GOES IR sensor was used in this study in order to attempt to quantify the amount of advection of the anvil particles from the main convective event directly due to affects of upper level winds. Data from the ER-2 CRS was used intermittently throughout as background information. Section 2 describes the process of cloud lifecycle break up as well as the calculations used for the anvil area extracted from

the GOES IR data. Section 3 describes the data collection of the wind profiles from the dropsondes and rawinsondes. Section 4 presents the results of the study followed by the discussion of error sources and future work in section 5.

2. Method of area extraction

The two cases used in this study were the storms viewed on July 19th 2002 (case 0719) and July23rd 2002 (case 0723) in southern Florida during the CRYSTAL-FACE campaign. These cases were chosen because of their near-complete data sets as well as ideal conditions for analyzing the affect of wind on an anvil cloud. The data from the GOES8-IR passive sensor brightness temperature (T_B) measurements at the 10.7μm band 4 wavelength was used in calculating the area of the anvil over time. The emmisivities of clouds in the IR are close to 1 equating approximately the brightness temperature to the actual temperatures of the clouds, excluding thin cirrus (Petty, 2004). A threshold of 230K was chosen to include only thick anvils found at or near cirrus levels. Cells were singled out and the pixels with T_B colder than the threshold were counted and converted to area in km^2 for each of the time retrievals. The area of each pixel is 14.5 km^2, a change in the x-direction of 3.065 km and a change in the y-direction of 4.012 km. A plot of the change in area for the case of 0719 can be seen in figure 2A and the same for the 0723 case in figure 3A.

An assumption is made that a single cell can be classified into three different lifecycle stages: the growth of the cloud due to convection, the expansion of the anvil by the upper level winds, and disintegration or death of the storm. As convection ensues, a steady decrease in T_B values over time would be observed and the time period of major convection can be determined; therefore, when the T_B appears to remain consistent over time, the assumption can be made that convection has ceased. A graph of the T_B for case 0719 can be seen in figure 2B and the same for case 0723 in figure 3B. The end of convection is represented by the green dashed line in figures 2 and 3. The rate of expansion, which can be determined by the change of area over time, for case 0719 and 0723 are shown in figure 2C and 3C respectively. The expansion rates will show negative results in the case of a dying cell. The time of major dissipation is marked by the red dashed line in figures 2 and 3. A fairly constant expansion of the anvil area can be

witnessed after the convection ends and before the major dissipation begins; this can be directly attributed to the speed and direction of the upper level winds near the cloud top.

3. Dropsonde and rawinsonde data to extract the upper level winds

In order to quantify the effect that winds have on the advection of particles away from the convective core, we must look only at the second stage of the cloud lifecycle: the expansion of the anvil due to the upper level winds. This is the only stage that has very little influence by any other external forces except the upper level winds during the expansion; although, this theory holds true only if the cloud top is not near the tropopause. Sounding data show that the tropopause for the 0719 is found at approximately 16.5km from the ground and subsequently at a height of 15.5km for the case on the 0723. The vertical cross sections from the CRS atop the ER-2 show the cloud tops for 0719 do not reach past a height of 14km (figure 4) or past a height of 15km for 0723 (figure 5). Thus, the two cases chosen, 0719 and 0723, show very little influence by the tropopause at the cloud levels that can be viewed by the GOES IR sensor.

The horizontal winds used in this study were taken from the NASA ER-2 high altitude research aircraft dropsonde measurements as well as the frequent Rawinsonde measurements from the Miami and Key West, Florida locations. For 0719, four dropsondes with wind speeds plotted in meters per second and directions in degrees from North were used and are shown in figure 6. Nine rawinsondes for 0719 are shown in figure 7 and were also plotted in meters per second and degrees from North for the wind speeds and wind direction respectively. The location of the dropsondes as well as the rawinsondes for case 0719 are shown on the map relative to Florida and the ER-2 flight track shown in figure 8; the dropsondes are shown as white dots while the Miami and Key West rawinsondes are shown as magenta dots. For 0723, three dropsondes with wind speeds plotted in meters per second and directions in degrees from North were used and are shown in figure 9. Eleven rawinsondes for 0723 are shown in figure 10 and were also plotted in meters per second and degrees from North for the wind speeds and wind direction respectively. The location of the dropsondes as well as the rawinsondes for case 0723 are shown on the map relative to Florida and the ER-2 flight track shown in figure

11; the dropsondes are shown as white dots while the Miami and Key West rawinsondes are shown as magenta dots.

4. Results

The 0719 case had average upper level winds at and between 15m/s and 18m/s from the dropsondes and 10m/s to 15m/s in the Rawinsonde data. The results show an area increase of 2183.7 km^2 with an average expansion rate of 0.681 km^2/s during the time period between the end of convection and the beginning of the major dissipation. These results can be found in figures 12A and 12B respectively. The case of 0723 had upper level winds clocked between 4m/s and 8m/s from the dropsondes and 9m/s to 13m/s in the Rawinsonde data. The results for this case show an area increase of 1619.7 km^2 with an average expansion rate of 0.676 km^2/s. These results can be found in figures 13A and 13B respectively. Little dispersion of the particles off of an easterly direction was found due to the consistent wind directions with height.

5. Discussions and future work

The expansion rate and subsequent area increase can directly be attributed to the wind speed and direction at upper levels in the anvil cloud during a time of ceased convection and prior to the major dissipation of the cloud. It is also important to note that the amount of particles being convected into the upper troposphere as well as the size of those particles have an affect on the length of time an anvil cloud persists and the area it covers. The current study conducted took into account only those particles large enough to be seen by the GOES IR sensor and CRS mounted on the NASA ER-2. Although these instruments give a good estimation of the expansion of an anvil over time, it by no means encompasses the entire visible anvil (especially the thin cirrus) and in effect will bias the radiative impacts of the cloud on the atmosphere. In order to combat these errors, a closer look will be taken at the combination of the CRS and CPL data set. This combination of data will allow the opportunity to view the smaller particles and thin cirrus located in the area. An example of the combination of the CRS and CPL data from the 0723 case, analyzed by McGill and Heymsfield et al., is shown in figure 14.

Other errors in the expansion calculations shown above come from the assumptions and approximations made at the beginning of the study. The expansion calculations were those that pertained only to the advection of the particles due to the upper level winds and the detrainment of the particles within the core were disregarded until more attention could be brought to the mass flux into the anvil.

The dissipation of the anvil cloud is also high in errors, mainly due to the difficulty in viewing small particles with the instruments used in this analysis. A basic model projection of the trajectories of four different sized particles was conducted to create a rough estimation of the fall times of particles within an anvil cloud with a similar wind profile as seen in cases 0719 and 0723. Explanation of this model is shown in appendix A. The results concluded that a particle with a diameter of 10μm will have a fall speed of approximately 0.014 m/s and therefore at a height of 15km near cloud top would remain in the atmosphere for ~ 300 hours or less traveling a distance of nearly 21,500km with a steady 20m/s wind behind it. Subsequently as shown in figure 15, a particle of diameter 50μm at a height of 14km will have a fall speed of 0.28 m/s remaining in the atmosphere for ~ 15 hours traveling a distance of 750km with a 15m/s wind behind it, a particle of diameter 100μm at a height of 13km will have a fall speed of 0.8 m/s remaining in the atmosphere for ~ 5 hours traveling a distance of nearly 200km with a 10m/s wind behind it and a particle of diameter 500μm at a height of 12km will have a fall speed of 4.5 m/s remaining in the atmosphere for less than 1 hour and barely traveling a distance of 10km with a 5m/s wind behind it. Although rough, this model projection supports the argument that smaller particles, invisible to the GOES and CRS instruments, will remain in the atmosphere longer and travel further distances from the main convective event.

References:

Beard, K.V., 1976: Terminal velocity and shape of cloud and precipitation drops aloft. *J. Atmos. Sci.,* **33**, 851.

National Aeronautics and Space Administration (NASA) Governmental Websites:

CALIPSO: <http://www.nasa.gov/mission_pages/calipso/spacecraft/index.html>

CRYSTAL-FACE: < http://cloud1.arc.nasa.gov/crystalface/ >

ISCCP: <http://isccp.giss.nasa.gov/overStatPg.html>

McGill, M., G. Heymsfield, D. Hlavka, L. Li, W. Hart and P. Racette: <http://cpl.gsfc.nasa.gov/Crystal/radarlidar/cplcrs.htm>

Petty, G.W., 2004: A first course in atmospheric radiation. Sundog Publishing. Madison, WI, pg 124-126, 143-146.

Wylie, D.P., W.P. Menzel, 1999: Eight Years of High Cloud Statistics Using HIRS. *J. Climate,* **12**, 170-184.

Stephens, G.L., D.G.Vane, D. TeBockhorst, S. Lini, 2008: CloudSat Colorado State Website <http://cloudsat.atmos.colostate.edu/instrument>

Yost C., P.Yang, B. Gao, B. A. Baum, M. King, S. Platnick, and P. Hubanks: A Comparison of MODIS and ISCCP Global Cloud Statistics. Poster Presentation.

Young, K.C., 1993: Microphysical Processes in Clouds. Oxford University Press. New York, NY, pg 174

Acknowledgements: I would like to thank Dr. Gerald Heymsfield and Lin Tian for their aid in this project as well as the Graduate Student Summer Program at NASA Goddard.

Appendix A. Particle Trajectory Model

To give a variety of sizes, 10μm, 50μm, 100μm and 500μm diameters were selected to analyze in the model trajectory run. The terminal fall velocities for these particles were extracted from a chart in K.C. Young, 1993. The terminal velocities calculated in the chart were for particles of the given sizes above of water drops in air at 0°C at 700mb based on Beard's 1976 treatment. Using this data is a large approximation for ice particles in an anvil cloud but was used because of the idea that the drag force as well as the geometry of a particle smaller than 500μm would not be too different for a spherical ice particle of the same size. Other atmospheric affects such as density differences in the air from a particle at 700mb as opposed to 300mb was neglected and the affects of turbulence, updrafts and downdrafts, sublimation and diffusion were also discounted due to complexity issues. These approximations will be revisited at a later date.

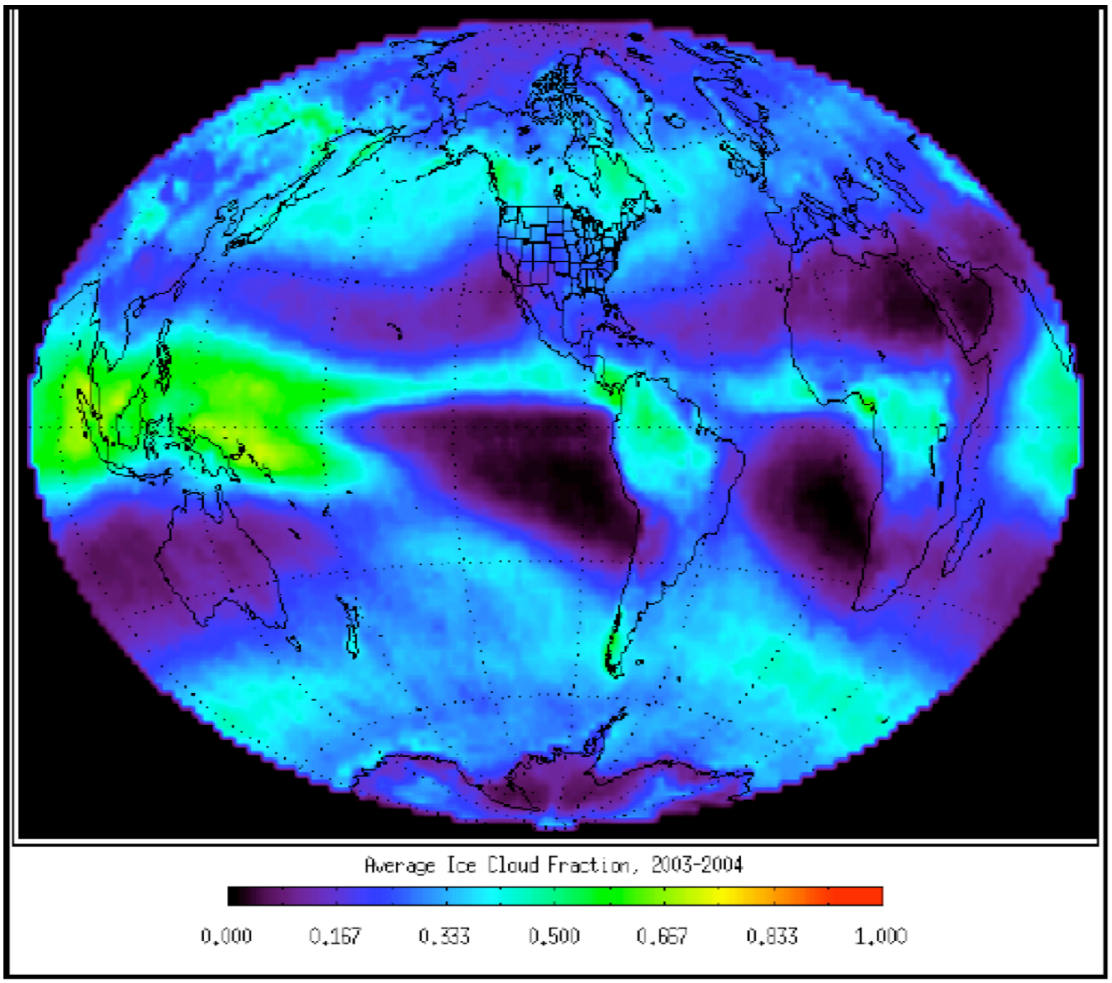

Figure 1. Average ice cloud fraction data derived by Yost et al. from the ISCCP data set.

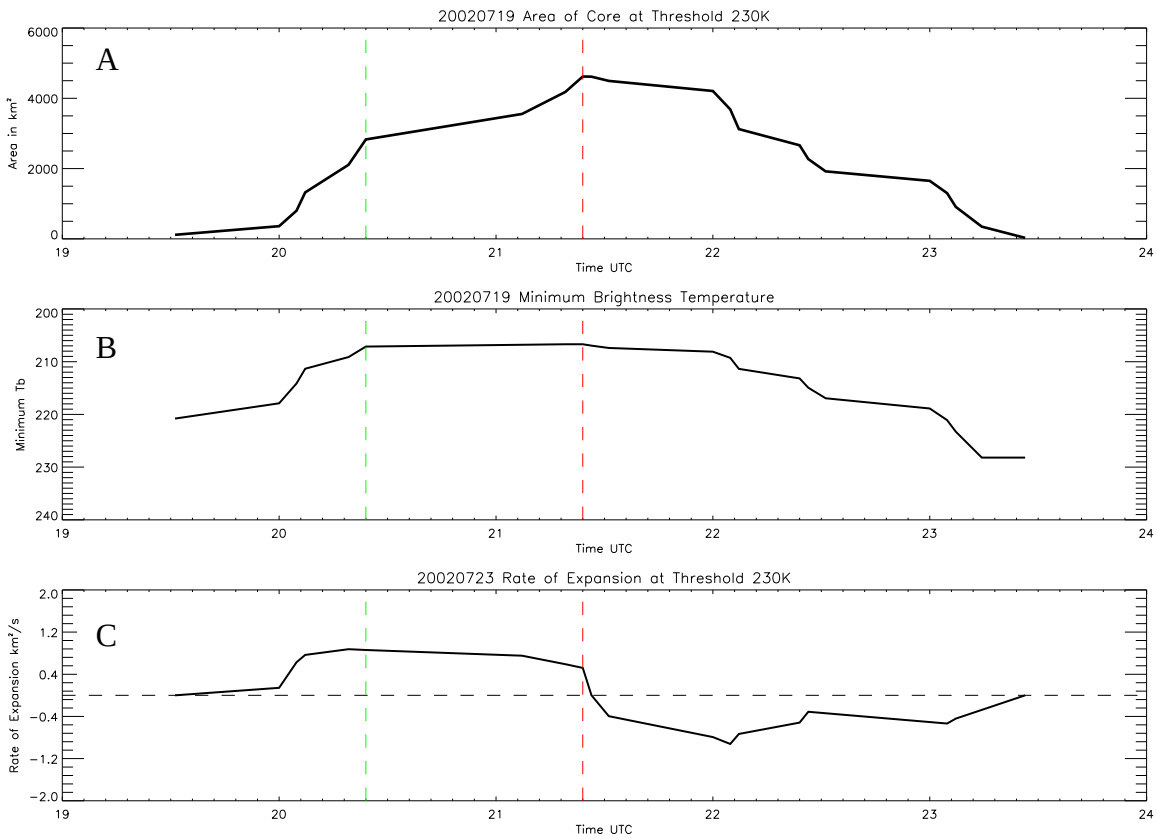

Figure 2. Case July 19th 2002 Southern Florida CRYSTAL-FACE campaign. A.) A plot of the area over time as calculated with the GOES IR sensor data. Green Line specifies the end of convection, red line specifies the beginning of the dissipation. B.) A plot of the minimum brightness temperature found in each GOES IR time frame. C.) A plot of the rate of expansion of the anvil over time calculated with the GOES IR sensor data.

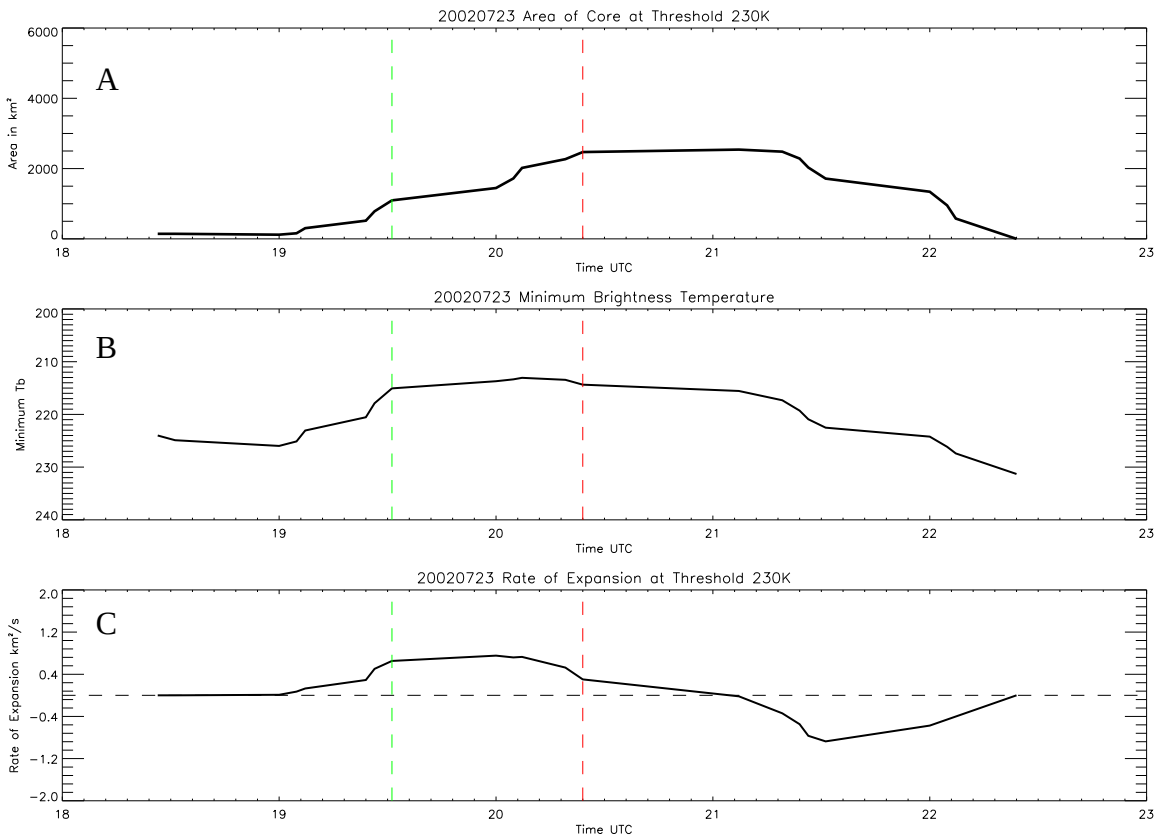

Figure 3. Case July 23rd 2002 Southern Florida CRYSTAL-FACE campaign. A.) A plot of the area over time as calculated with the GOES IR sensor data. Green Line specifies the end of convection, red line specifies the beginning of the dissipation. B.) A plot of the minimum brightness temperature found in each GOES IR time frame. C.) A plot of the rate of expansion of the anvil over time calculated with the GOES IR sensor data.

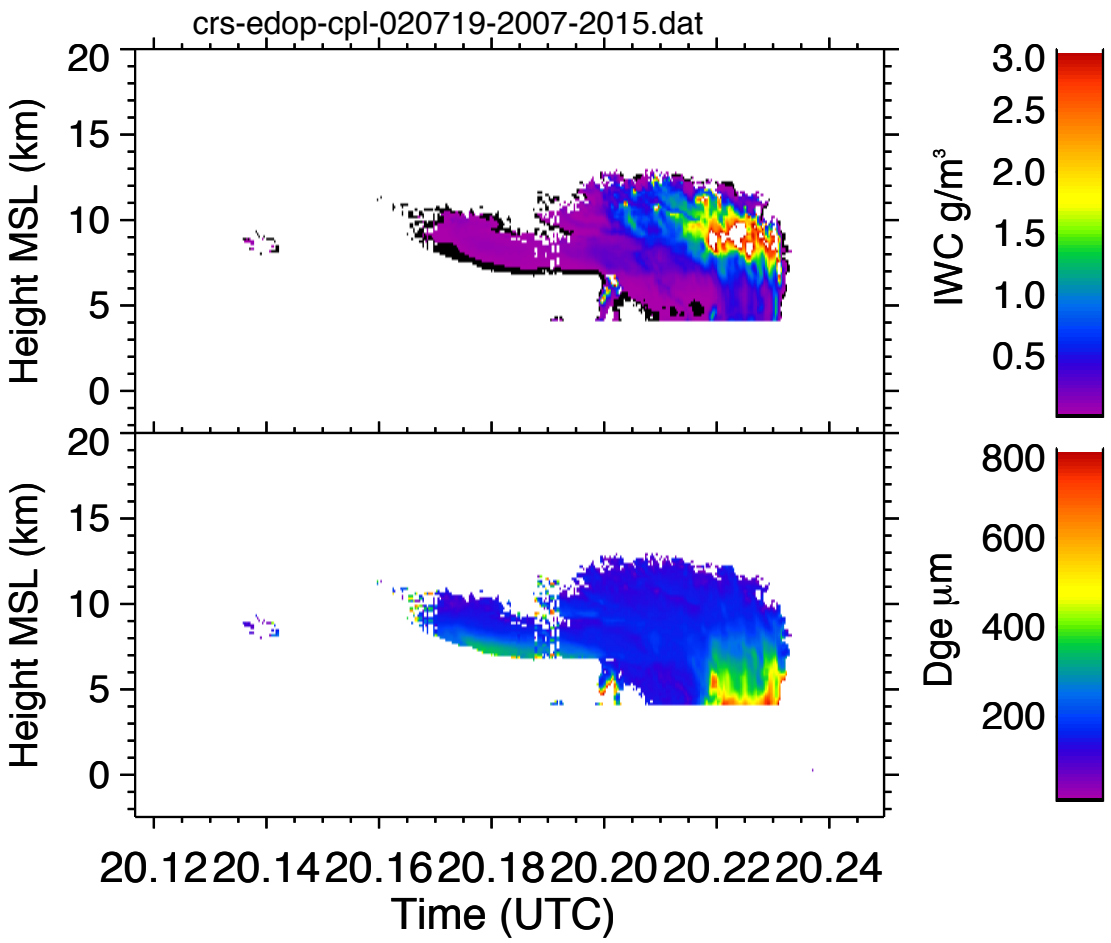

Figure 4. A vertical cross section from the NASA ER-2 CRS system during CRYSTAL-FACE for the 0719 case. Presented is the ice water content (IWC) in g/m^3 and the particle size distribution (Dge) in µm.

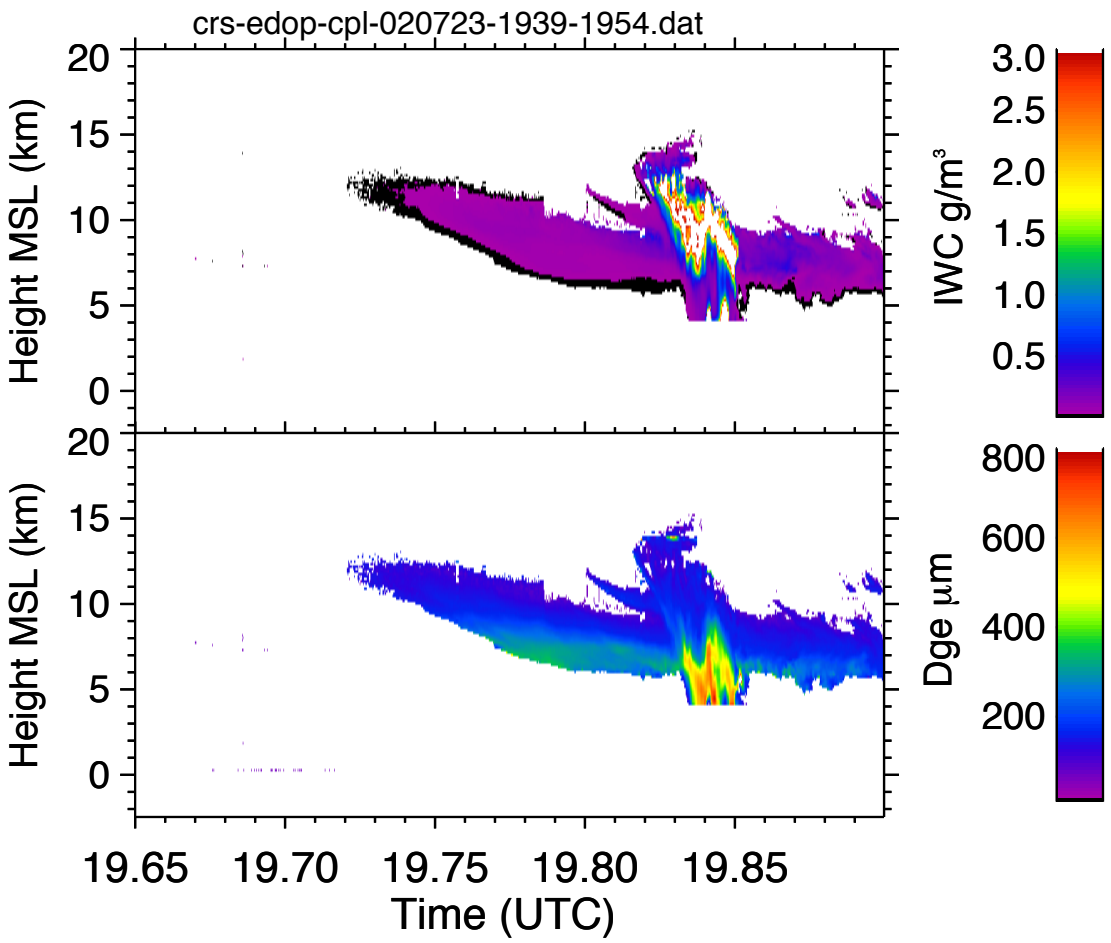

Figure 5. A vertical cross section from the NASA ER-2 CRS system during CRYSTAL-FACE for the 0723 case. Presented is the ice water content (IWC) in g/m^3 and the particle size distribution (Dge) in µm.

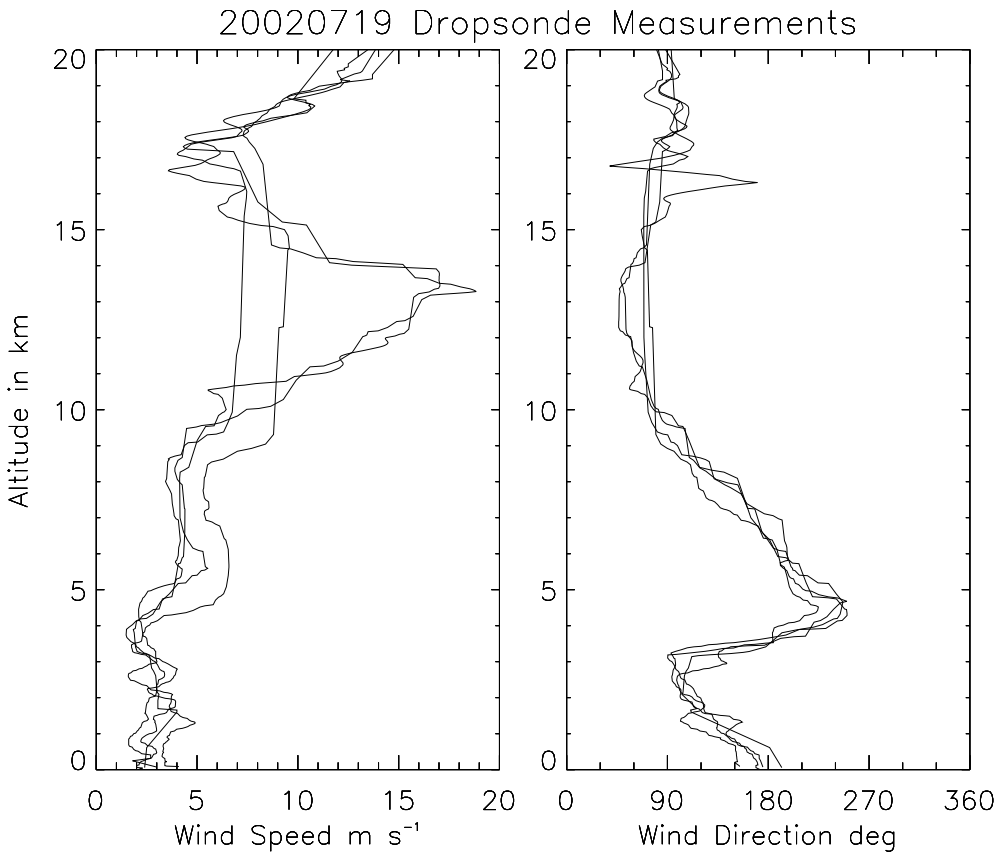

Figure 6. NASA ER-2 dropsonde measurements for case 0719. Wind speed in meters per second and wind direction in degrees from North.

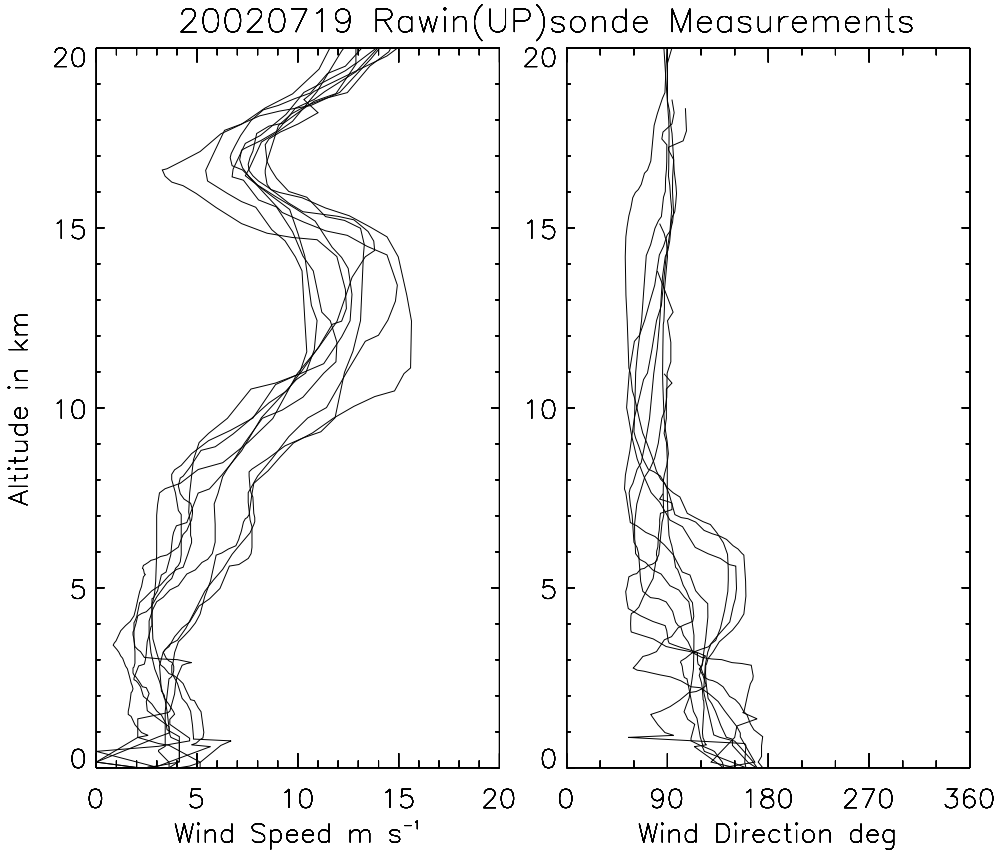

Figure 7. Rawinsonde measurements from Miami and Key West Florida for case 0719. Wind speed in meters per second and wind direction in degrees from North.

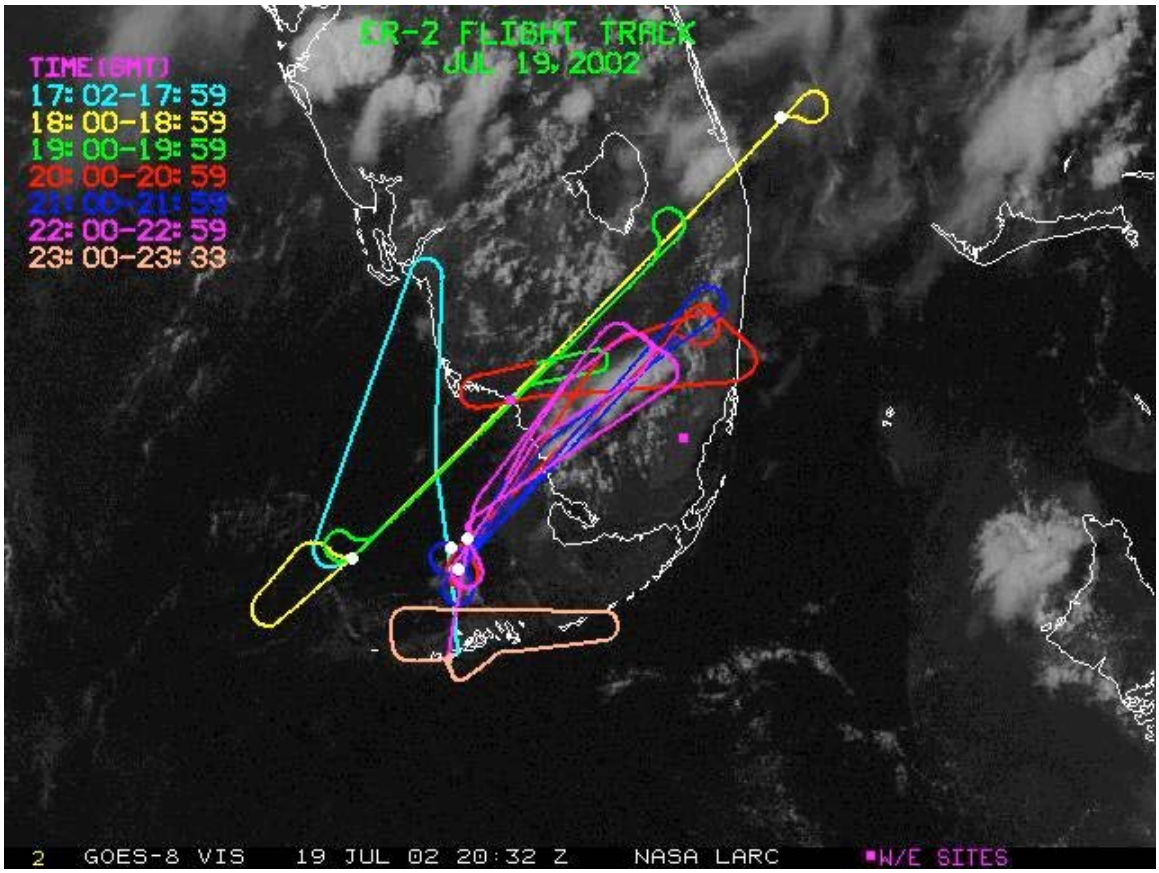

Figure 8. Case 0719 ER-2 flight path over southern Florida during the CRYSTAL-FACE campaign in 2002. White dots show placements of the ER-2 dropsondes, magenta dots represent the Miami and Key West rawinsonde launch sites.

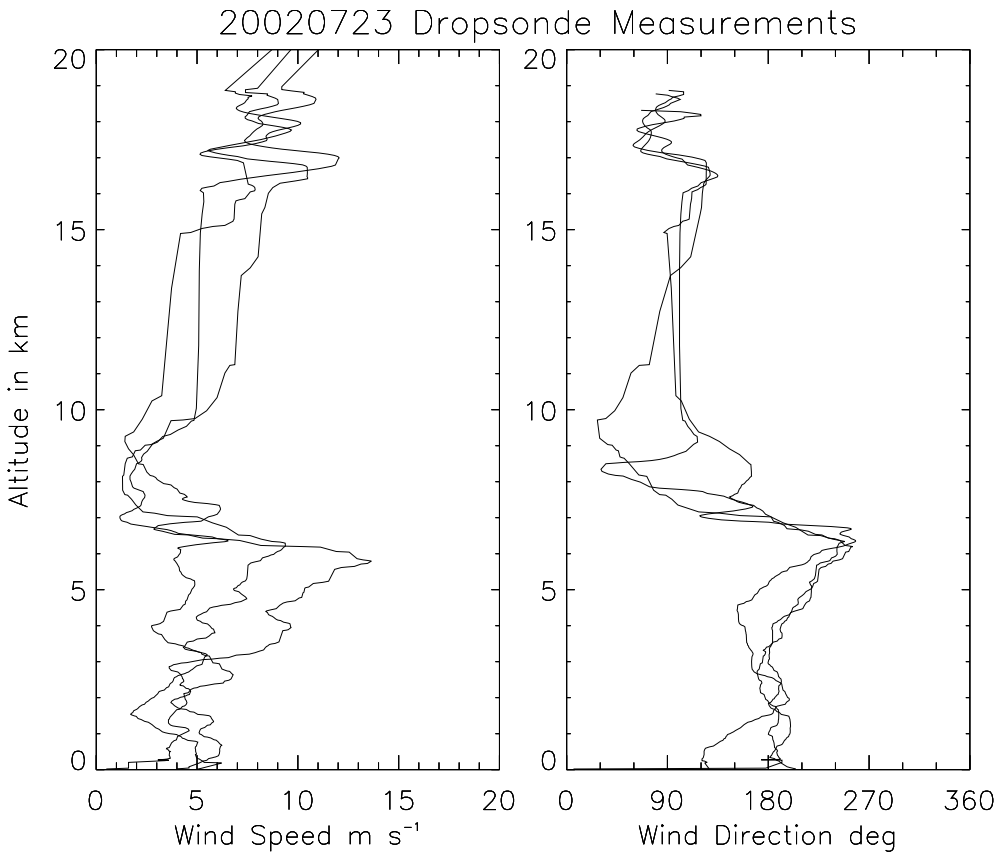

Figure 9. NASA ER-2 dropsonde measurements for case 0723. Wind speed in meters per second and wind direction in degrees from North.

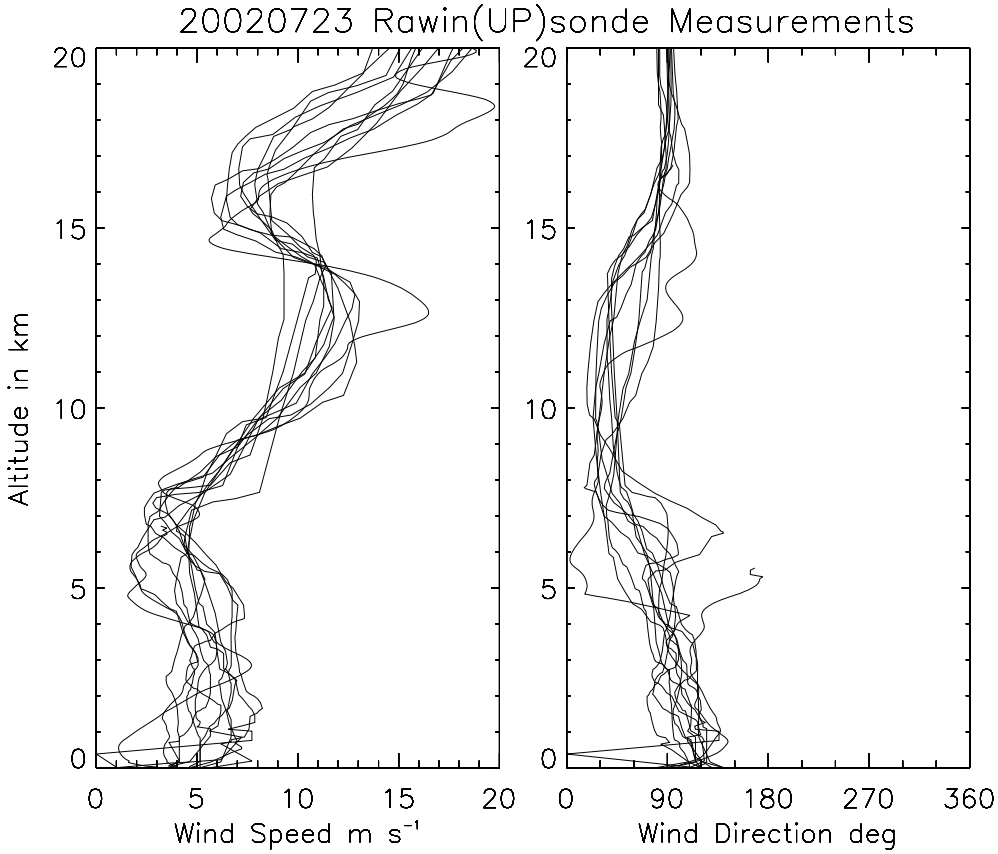

Figure 10. Rawinsonde measurements from Miami and Key West Florida for case 0723. Wind speed in meters per second and wind direction in degrees from North.

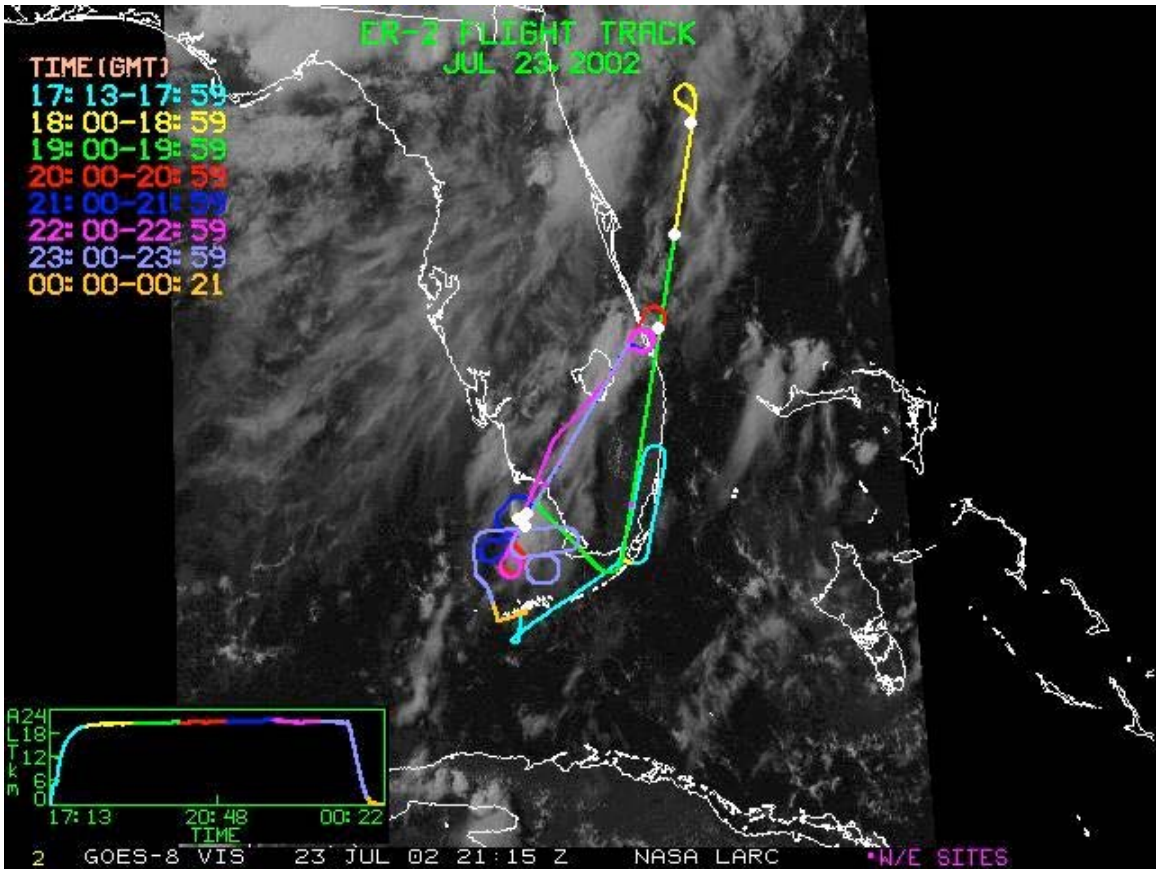

Figure 11. Case 0723 ER-2 flight path over southern Florida during the CRYSTAL-FACE campaign in 2002. White dots show placements of the ER-2 dropsondes, magenta dots represent the Miami and Key West rawinsonde launch sites.

A

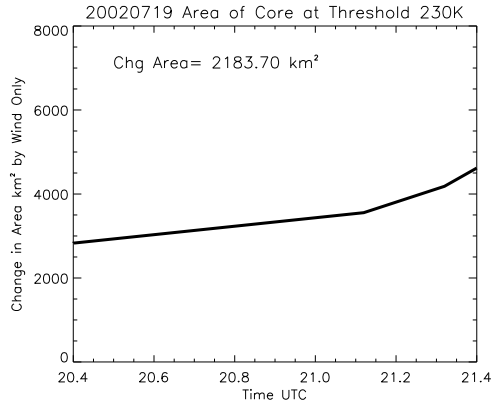

B

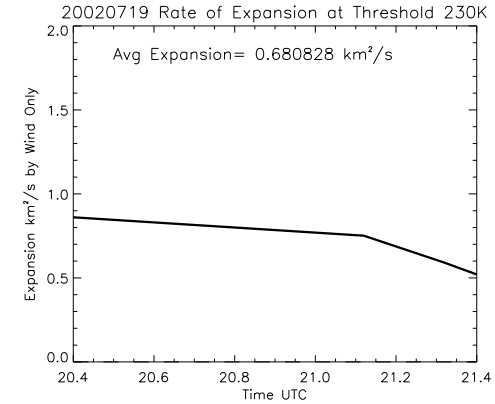

Figure 12. A.) Change in area in km^2 over time by the upper level winds only for case 0719; total area change 2183.7 km^2. B.) Expansion rate in km^2/s over time by wind only for case 0719; average expansion rate for wind only segment 0.680828 km^2/s.

A

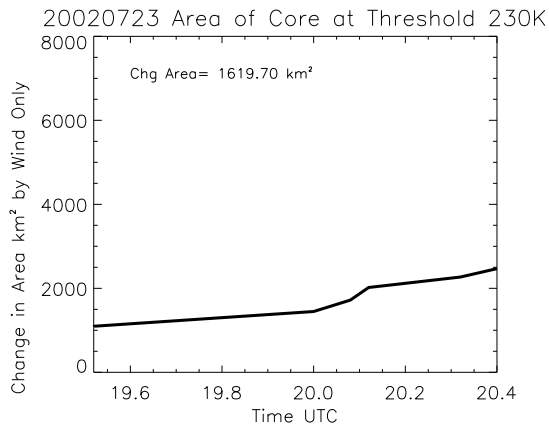

B

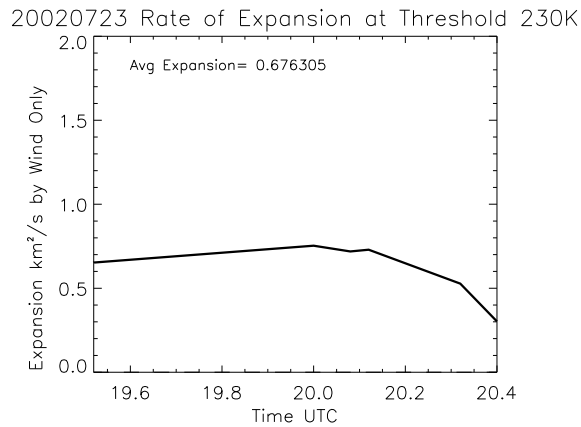

Figure 13. A.) Change in area in km^2 over time by the upper level winds only for case 0723; total area change 1619.7 km^2. B.) Expansion rate in km^2/s over time by wind only for case 0723; average expansion rate for wind only segment 0.676305 km^2/s.

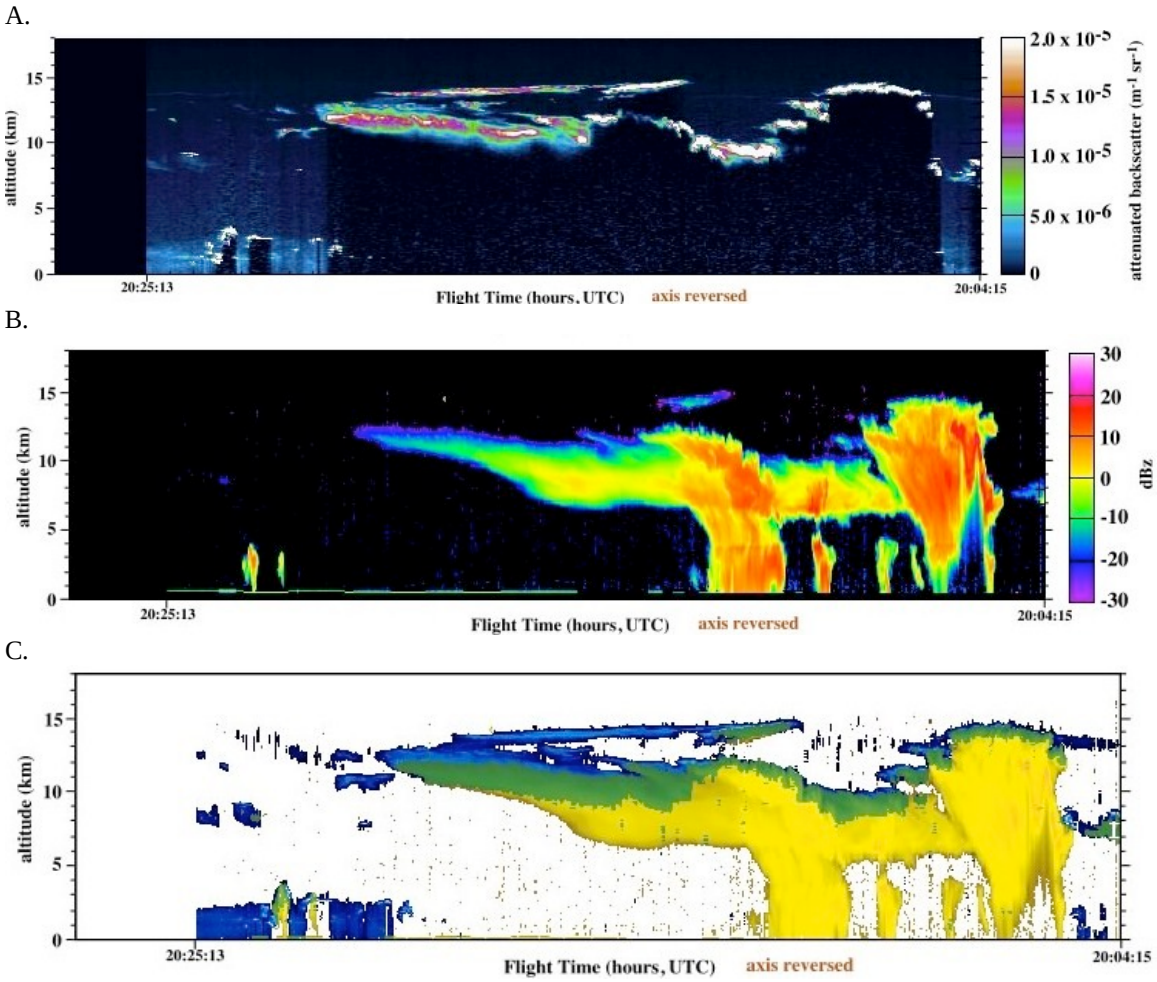

Figure 14. A.) CPL measurements for case 0723. B.) CRS measurements for case 0723. C.) Combined CPL CRS data set for case 0723. CPL data by M. McGill, D. Hlavka, W. Hart, CRS data by G. Heymsfield, L. Li, and P. Racette.

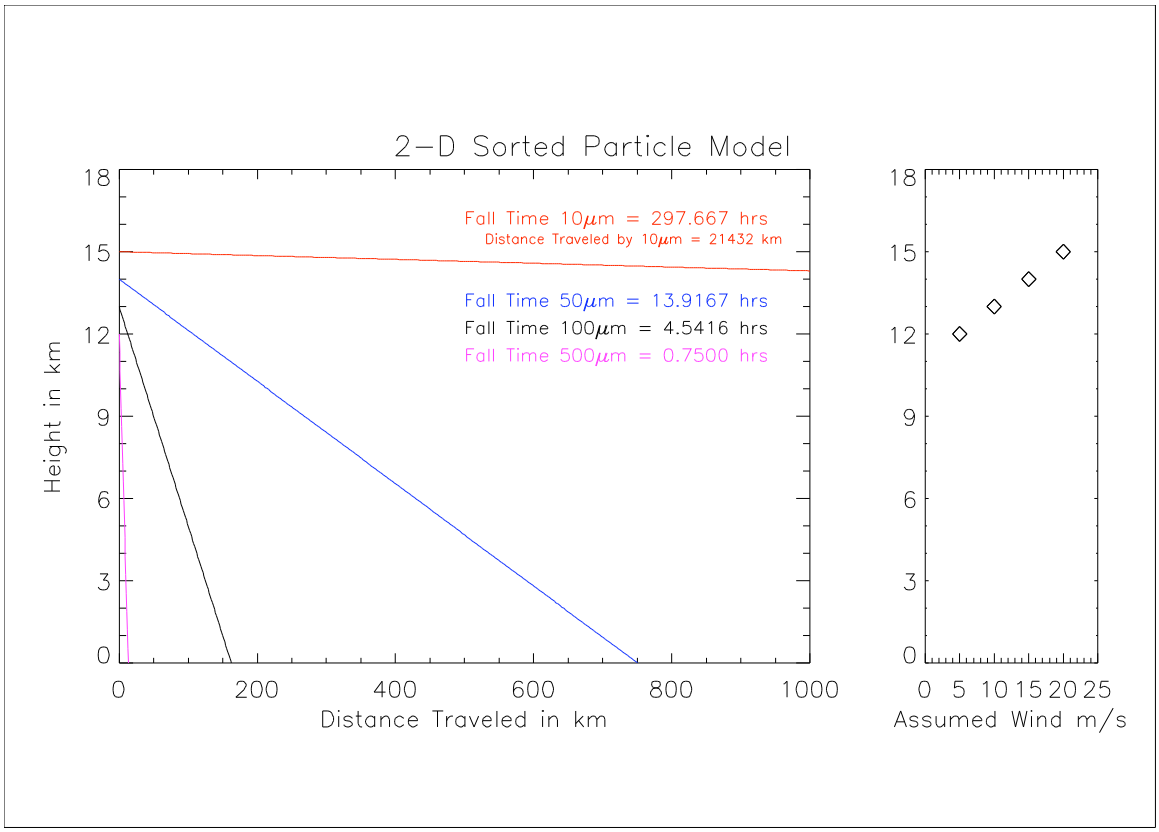

Figure 15. A basic particle model for 4 different sizes of particles: 10µm, 50µm, 100µm, 500µm. Wind profile is assumed linear with height based on wind profiles seen in cases 0719 and 0723. Approximations explained in appendix A.